CHAPTER 2

LITERATURE REVIEW

2.1 An Introduction to Ruby Stones

Gems like diamonds, rubies, sapphires, and emeralds have been valued for their color, transparency, brilliance, and durability for decades. They are also acknowledged as being stunning and having exceptional value (Wise, 2021). The ruby is a corundum combination (a-Al_2O_3), where a small amount; roughly 1%; of Cr3+ substitute Al3+ to yield a distinctive crimson color (Nassau, 2003). Rubies are red-colored gemstones that are hexagonal and treasured for their beauty. Large rubies are usually more expensive than diamonds as rubies are harder to obtain and are rarer than diamonds. Heat treatment accentuates the natural color of rubies and reduces the number of milky particles in the stone (Whitney, 2011). Natural rubies are some of the most precious gemstones in the world. It is very rare to acquire large-sized rubies with high clarity. These rubies are even more valuable than same-sized diamonds. The carat, color, beauty, and origin of a ruby determine its market value. Rubies have traditionally been mined in the Far East, while Afghanistan, Burma (or Myanmar), Cambodia, India, Madagascar Sri, Lanka, Tanzania, Thailand, Kenya, and Vietnam are the leading suppliers. However, for decades, the global supply of rubies has come from two regions; modern-day Sri Lanka and Myanmar, specifically Mogok. From the late 1800s through the 1990s, the border region of Thailand and Cambodia produced high-quality diamonds; however, this was noted only during the 1960s (Tang et al., 1988).

2.2 Application of Ruby Stones in the Industry

Rubies have a long history, and both synthetic and natural rubies have a wide range of applications in modern society. Rubies are widely used in jewelry, where they are set in valuable metals, such as platinum or gold. They can be utilized as the focal point of a piece or to complement other gemstones, such as diamonds. As rubies are extremely hard, they are easy to care for and virtually impervious to nicks and cracks from everyday wear and tear (Issa & Brabazon, 2021). According to Ferns Icon (n.d.), if one was to wear a ruby, the gem should ideally weigh at least 1/10th of the wearer's body weight in carats. Therefore, someone weighing 70 kg should wear a gem of at least seven carats. This translates to approximately three to five grams in weight. Figure 2.1 provides a picture of a ruby jewellery set.

Source: https://www.pinterest.com/kiranmaimadadi/ruby-necklace/

Figure 2.1: Ruby Jewellery Set

The moving parts of various gadgets rely on bearings, little balls that move or rotate particular sections of a machine; for flexibility. Ruby bearings are often used if friction is a problem. Although rubies are smoother than most metals and produce less

friction when used as bearings, the cost of a gadget increases when rubies are used (Ferns Icon, n.d.).

Jewel bearings are commonly employed as the moving parts of mechanical watches as they prevent friction, wear, and tear among mechanical parts due to their toughness and rigidity. Jewel bearings' benefits include precision, small size, low weight, predictable friction, exceptional thermal stability, and lubrication-less performance for decades (Naas, 2013). The complexity of the movements required determines the number of rubies in a mechanical watch; i.e., more rubies are required when there are more moving parts. A typical fully jeweled time-only watch has 17 jewels. However, watches can contain many more jewels. Figure 2.2 depicts the use of rubies as bearings in a mechanical watch.

Source: https://en.worldtempus.com/article/watches/innovation-and-technology/watch-education-understanding-the-use-of-rubies-13737.html

Figure 2.2: Rubies in A Mechanical Watch

Scientists have recently used rubies in laser technology due to their ability to focus light and produce a higher intensity than most gemstones. Like diamonds, rubies can transmit light from one point to another with low-energy waste. As such, they are

frequently a key component in precision lasers. In their study, Maiman (1960) developed the first ruby laser that could be used for commercial purposes. The ruby lasers consist of aluminum oxide (Al_2O_3) as a host, while Cr3+ (triple-ionized chromium ions) acts as a lasant. This laser shows an output wavelength of 0.6943 nm and operates in a pulsed mode. A flash lamp that gives a capacitive discharge is needed as an excitation medium.

Ruby lasers have a red tone and are commonly employed in the military and in range-finding equipment for surveying purposes. A solid-state laser is used for high-power tasks, such as welding, cutting, drilling, and molding (Whitney, 2011). Ruby lasers can be used for spot welding, drilling diamonds, sending mood pulses, hole piercing, and pulsed holography, as it releases a lot of energy (several Joules) in one pulse (Hung et al., 2019). However, unlike many other solid-state lasers, rubies provide remarkable laser light emissions (Whitney, 2011). This is also the reason why many commonly associate the color red with lasers (Raymond, 2016). Ruby solid-state lasers have significantly more benefits than gas lasers (RF Wireless World, n.d.). Firstly, the beam diameter of a ruby laser is smaller than that of a carbon dioxide (CO_2) laser. The power output of a ruby laser is also comparable to that of a helium-neon (He-Ne) laser. Furthermore, as rubies are solid, there is no risk of wasting active medium material.

Fok et al. (2017) examined ruby laser treatments to remove and fade grayish-brown pigmentation patches from the skin of 40 patients (Fok et al., 2017). A Q-switched 694nm ruby laser (QSRL) at an energy density of 8–10 J/cm^2 could clinically fade pigmentation on human skin. Figures 2.3 and Figure 2.4 present the real-time monitoring using photothermal images, of the plots depicting the patient's facial skin temperature before and after the Q-switched ruby laser treatment.

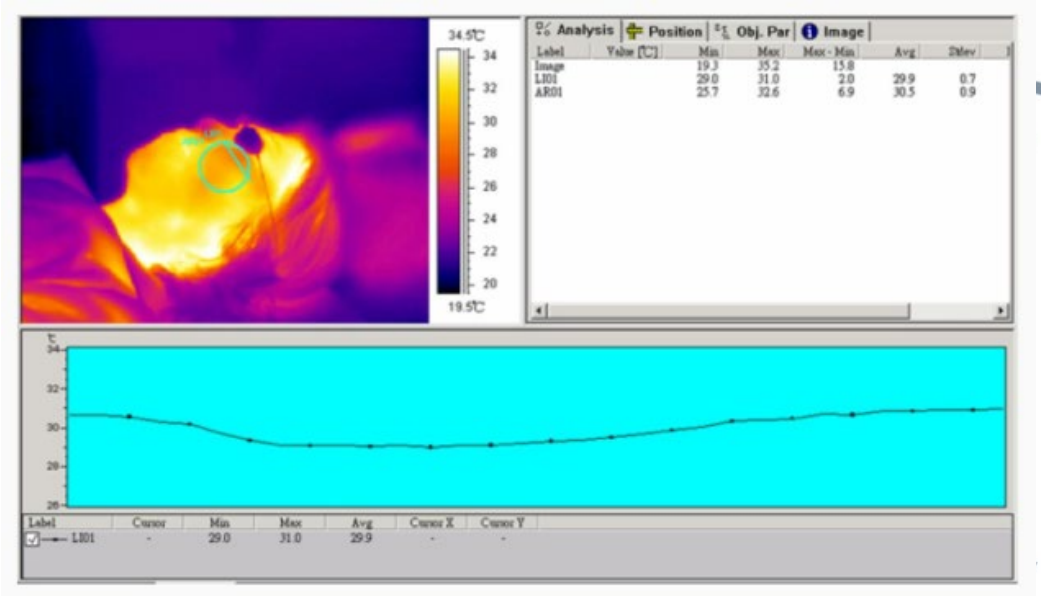

Source: Fok et al. (2017)

Figure 2.3: Plot Depicting the Patient's Facial Skin Temperature Before The Q-Switched Ruby Laser Treatment for The Nevus of Ota Using an Infrared Thermal Image Apparatus

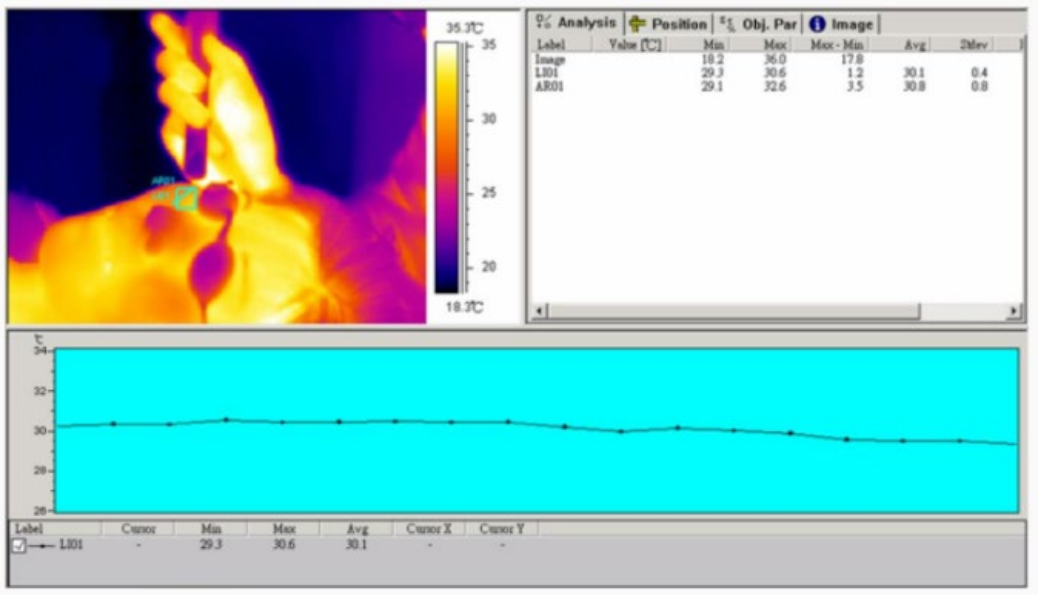

Source: Fok et al. (2017)

Figure 2.4: Plot Depicting the Patient's Facial Skin Temperature 15 S After The Q-Switched Ruby Laser Treatment Carried Out Using an Energy Density Of 9 J/cm^2

Figure 2.5 depicts the results of a 19-year-old female after four QSLR treatments over two years. The results showed an excellent cleaning and fading response. Therefore, due to the diverse uses for ruby stones in various industries; such as jewelry, bearings, welding, and medical; it is important to have a standardized method of grading ruby stones. This is because these standardizations will facilitate the effective utilization of these gemstones in the relevant industries. Therefore, this present study proposed producing a conceptual model to grade ruby stones quantitatively using CCD tomography.

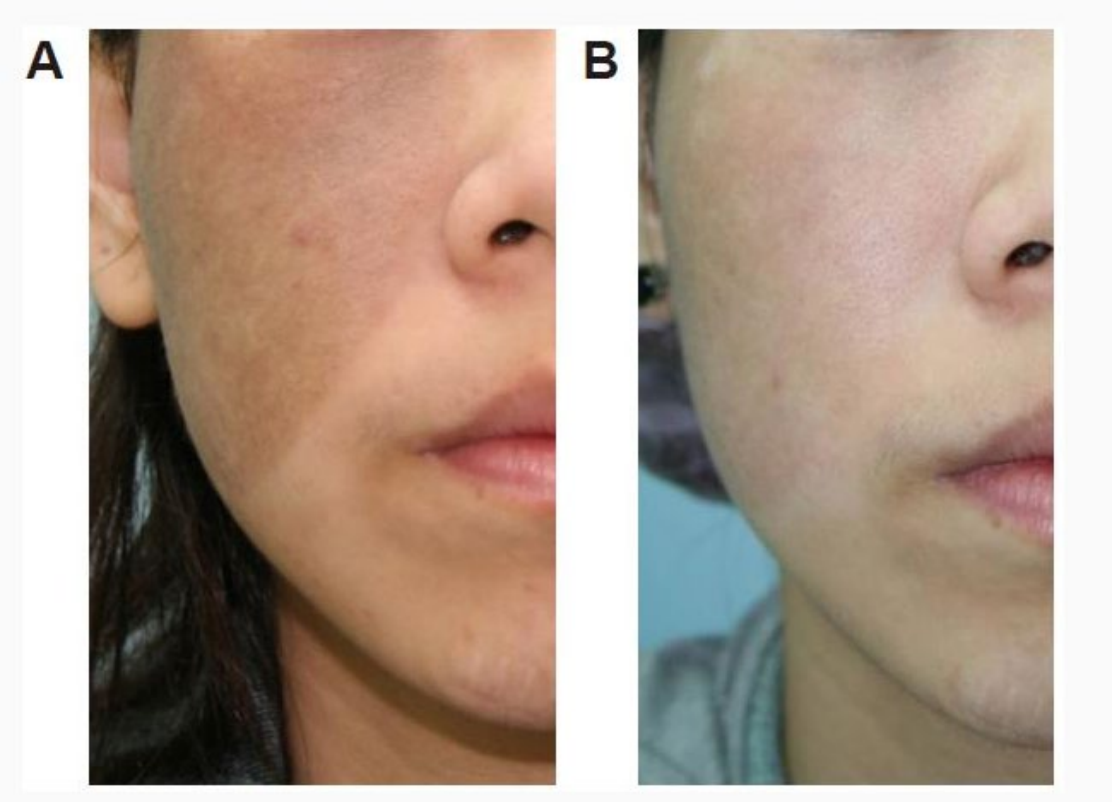

Source: Fok et al. (2017)

Figure 2.5: A 19-Year-Old Asian Female Having Nevus of Ota on Her Right Cheek: (A) Before Laser Therapy; (B) 2 Years After 4 Treatments Using The Q-Switched Ruby Laser (694 nm) at an Energy Density Of 9-10 J/cm

2.3 Characterisation of Ruby Stones

Although no two diamonds are the same, they all have some features that affect their values. 4Cs categorize the properties of a diamond; carat weight, clarity, color, and cut; are the properties of a diamond (Diamond Council of America, 2014). However, how each aspect affects the cost varies from one type to the other (Leelawatanasuk et al., 2014). For example, yellow sapphires have higher clarity than the average blue sapphire, and blue sapphires have a higher clarity than the average ruby. As a result, clarity flaws in rubies have a lower pricing influence than flaws in blue sapphires.

2.3.1 Clarity

Inclusions, substances trapped within the gem, are used to grade the gemstone's purity. Nevertheless, viewing inclusions can be difficult. Gemologists often use a microscope to study them, preferably with darkfield illumination. While a magnification of 30–60X (the range of most stereoscopic microscopes) may resolve many inclusions, some tinier ones require magnification of 200X or more. Knowing how to use your microscope and various lighting techniques is essential for identifying inclusions. However, in some cases, getting tiny details into sharp focus often proves quite challenging, if not impossible. Sometimes, student gemologists can easily jump to conclusions about what they see through magnification.

The clarity grade of a gemstone denotes the absence of some materials trapped within the gem, such as inclusions, flaws, or surface fissures, which impact its final appearance and total surface area. Rubies rarely exhibit the high clarity of fine diamonds. When viewed at 10x magnification, even the best rubies are likely to have inclusions. However, a ruby with no imperfections should be regarded with caution as

it may be a synthetic stone or a glass imitation. Inclusions come in nine different varieties and are common in rubies. The inclusions that could be seen in diamonds are analogous to needles, crystals, cavities, twinning, and feathers. However, the frequently encountered inclusions unique to rubies are silk, fingerprints, scratches, and color zoning.

2.3.1.1 Silk

The silk structure of a ruby reveals a lot about its treatment history, as rubies are often heated to change their color or improve clarity. However, the strong heat used to treat rubies partially melts or decomposes its silk, and perfect silk indicates that the ruby was not heat-treated. In contrast, degraded silk (primarily visible in a magnified image and recognized by an expert gemologist) shows that the ruby stone was subjected to heat treatment (Walter, 2021). Figure 2.6 shows a deep red cabochon ruby with a perfect six-rayed star, which indicates that the stone has not been heat-treated.

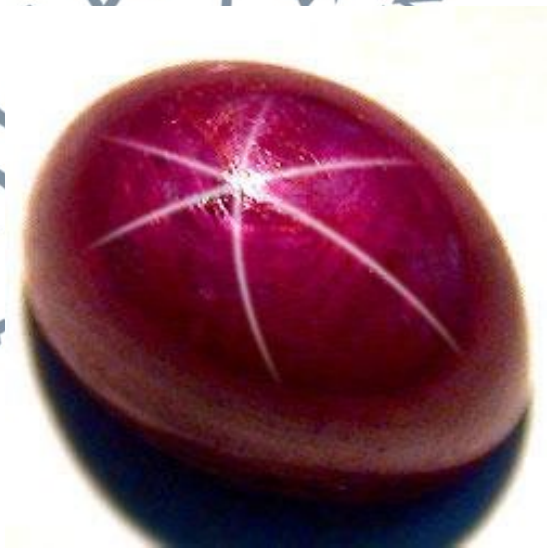

Source: Walter (2021)

Figure 2.6: A Deep Red Cabochon Ruby with A Perfect Six-Rayed Star

2.3.1.2 Fingerprint

Fingerprints are incredibly common in sapphires and rubies because they are evidence of fractures occurring and healing in the stone naturally. Many stones cannot heal their fractures, like emeralds. While this is a naturally-occurring inclusion, synthetic rubies can show fingerprints, too, because this is a specific characteristic of the corundum mineral and not its inclusions (Walter, 2021). Fingerprints are inclusions that are clustered together and quite literally can look like human fingerprints. These inclusions are typically small and rarely impact the quality of a ruby. Figure 2.7 below shows the fingerprint inclusion of rubies.

Source: Walter (2021)

Figure 2.7: Fingerprint Inclusion of Rubies

2.3.1.3 Scratches

An original ruby is not easily to scratch; the corundum family is one of the strongest types of stone. Composite rubies have the drawback of including glass, making them vulnerable to chemical damage from cleaning products and easy to fracture. One practical test to validate the originality of ruby stone is by scratching the

surface of the ruby by using nails or any other stuff that is neither a diamond nor moissanite. Only a real gemstone with a higher Mohs rating could scratch other gemstones (Walter, 2021). Figure 2.8 below shows an example of a scratched ruby.

Source: Walter (2021)

Figure 2.8: Picture of a Scratched Ruby

2.3.1.4 Color Zoning

Common in all corundum varieties, color zoning is a concentration of color in different parts of a stone. Sometimes cutters take advantage of color zoning to display color in parts of the stone that do not have any. Color zoning in corundum can produce multicolored stones like particolored tourmalines, sometimes called particolored sapphires. If this were to happen to a ruby, it would only qualify as a ruby if red accounts for more than 50% of the stone's color. Figure 2.9 below shows the blue color zoning observed in some of the unusual rubies; immersed in methylene iodide.

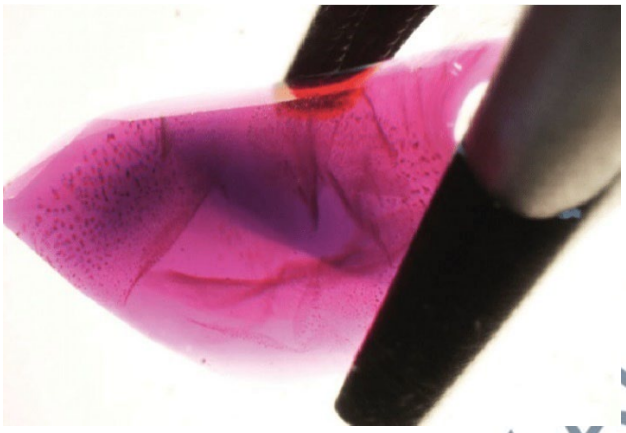

Source: Walter (2021)

Figure 2.9: Blue Color Zoning in Ruby

2.3.1.5 Grading of Ruby Stone Based on its Clarity

The ideal clarity grade for ruby is called "eye-clean." This means that there are no apparent inclusions to the human eye. The more transparent a star ruby is, the more valuable it is (Renfro et al., 2018; Walter, 2021). The size, number, location, and overall visibility of the inclusions are essential aspects that an expert considers when evaluating a ruby stone's clarity. There are different clarity criteria for opaque and translucent gemstones compared to clear gems. Figure 2.10 below shows the different grades of ruby stones according to clarity.

Source: https://www.withclarity.com/education/gemstone-education/ruby/ruby-grading

Figure 2.10: Different Grades of Ruby Stones According to Clarity

As all other criteria; such as carat (weight), colour, and cut; are equal, rubies are priced according to their clarity grade (Table 2.1), where I indicates inclusion, SI denotes slight inclusion, VS indicates very slight inclusion, and VVS denotes very, very slight inclusion (Grande & Augustyn, 2010).

Table 2.1: Price of Ruby Stones According to Clarity Grade

Level of Clarity (Grade)	Quality of Rubies	Price Per 1 Carat (Dollar, $)
(I)	Very low	20
(I-SI)	Low	30-40
(VS)	Good	50-60
(VVS)	Very good	100-110

Source: Grande & Augustyn (2010)

Based on all these criteria or the quality of the gemstone, this present study will focus on clarity to establish a optical properties of ruby stones using CCD tomography. The CCD sensor's superior performance will be explained in the literature review. Extant studies have found that CCD tomography can effectively identify an object's varying transparencies (Jamaludin & Abdul Rahim, 2016). Therefore, the clarity of ruby stones will be the main subject of this present study as it is difficult to detect the inclusion or materials trapped within rubies with the human eye.

2.4 Gemmology Tools for Gemstone Characterisation

A ruby stone is graded and valued based on color, transparency, and blemishes. Several Gemology tools have been developed for determining the optical characteristics of synthetic and non-synthetic ruby stones, like a loupe, microscope, and dichroscope

(Liao et al., 2017; Mukherjee, 2012). However, all these tools depend on human visual assessment, where the assessor needs many years of experience. However, all these techniques are not standardized and can lead to inaccurate grading valuation as they depend on graphical inspection (Liao et al., 2017; Mukherjee, 2012).

Multiple gemstone-related studies have conducted different types of research on gemstone characterization. In one such study, Yu et al. (2019) stated that the gemstone's chemical and physical characteristics and inner structures can be generally analyzed by polarizing microscopy, microscopic observations, and Raman spectroscopy. Here the light reflected off the region on the gemstone, when illuminated by a point light, forms a bright light band on the convex gemstone. However, this methodology is inaccurate and relies on the inner structure of the gemstones, making it an unreliable and inconsistent technique.

A few researchers (Abduriyim & Kitawaki, 2006; Sutherland et al., 2019) employed the LA-ICP-MS (laser Ablation–Inductively Coupled Plasma–Mass Spectrometry) technique for identifying the elemental composition of particular gems to pinpoint their origin geography. Sutherland et al. (2019) determined the age of the rubies using the uranium-lead (U-Pb) isotopes in the titanite inclusions (Thurein Taung; 32.4 Ma) and the zircon inclusions (Mong Hsu; 23.9 Ma) and basalt dating in New South Wales (NSW) (>60–40 Ma). This claim could be tested after analyzing the ruby stones acquired from Mong Hsu, Thurein Taung, and Mogok. The researchers compared the data collected from New England and East Australia with that collected from the proposed Mong Hsu field, as shown in Figure 2.11.

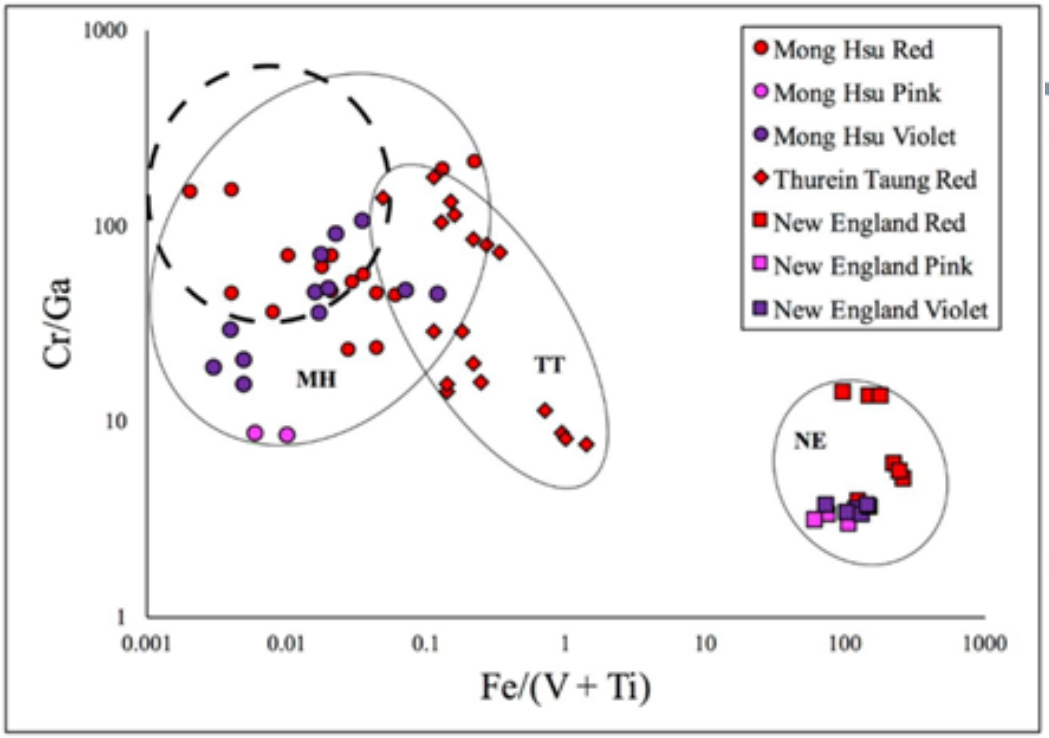

Source: Sutherland et al. (2019)

Figure 2.11: Ruby Plots of Stones Obtained from Mong Hsu (MH), Thurein Taung (TT), Myanmar, and New England, East Australia (NE) Were Presented in The Oval Enclosing Field Boundaries in The Cr/Ga Vs. Fe/ (V + Ti) Diagram. All Plots Were Colour- And Locality- Coded for Describing the Multi-Zoned Crystals

Abduriyim & Kitawaki (2006) noted that using the LA-ICPMS technique was very effective in geology, Gemology, geology, and materials science as it presents an efficient analysis and does not require any sample preparation. The LA-ICP-MS analyses offer a lot of quantitative data for detecting the presence of major, minor, and trace elements in the analyzed samples, which help design variation diagrams and "chemical element fingerprints." These fingerprints highlight variances between samples, attributable to geographic location or sample treatment. Figure 2.12 depicts the instrumentation of the LA-ICP-MS.

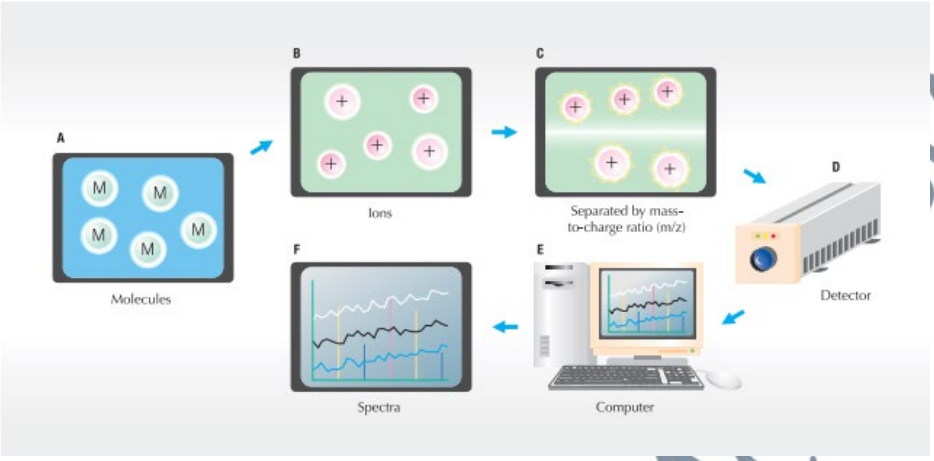

Source: Ahamdjan Abduriyim & Kitawaki (2006)

Figure 2.12: A Graphical Depiction Describing How the Mass Spectrum Is Generated by A Sample. In This Process, The Gaseous Molecules of Sample (A) Are Ionized and They Form Gaseous Ions (B). These Ions Are Passed Through the Mass Analyser (C) And Are Separated Based on Their Mass-To-Charge Ratio and Then Passed to The Detector (D). Thereafter, Computer (E) Transforms the Signal Generated from Every Element into The Spectrum That Is Presented on The Computer Screen (F)

However, the above-mentioned established measurement techniques cannot offer a standard grading of the ruby stones. Some researchers have used the LA-ICPMS technique to determine the elemental composition of certain gems for the origin of geography. Breeding et al. (2006) used high-energy ultraviolet luminescence to process gemstone images. Over the decades, gemologists have discovered that genuine and laboratory-grown gems react differently to UV radiation because the treatments frequently alter fluorescent reactions. The standard hand-held UV lamps can be effectively used for observing the bulk fluorescence colors and the distribution patterns of gemstones; however, they do not reveal weak or intricate patterns within the stones.

The DiamondView™ device, manufactured by the Diamond Trading Company, induces fluorescence in diamonds and reveals growth patterns that help distinguish natural stones from synthetic ones using very high-energy ultra-short-wave (230 nm) UV radiation. Figure 2.13 shows the DiamondView™ device.

Source: Breeding et al. (2006)

Figure 2.13: DiamondView™ Instrument

The device uses a high-resolution camera with aperture and exposure-adjusting abilities to digitally capture even the weakest luminescence. The high-energy UV imaging capabilities of the DiamondView™ can do more than identify synthetic diamonds when paired with gemological observations or high-tech spectroscopic investigations such as laser-induced photoluminescence. However, this framework can only differentiate and analyze the originality of gemstones, whether artificial or natural, which is not a quantitative grade in the valuation of rubies.

Imaging spectroscopy, developed in 2006, is used to distinguish gemstones in terms of color intensity (Del Re, 2006). As presented in Figure 2.14, a triangle (soc figure) can be used to represent the pillars of the hyperspectral imaging system. These include different instruments like imagers, spectrometers, and radiometers that capture the gem stones' spatial, spectral and intensity data.

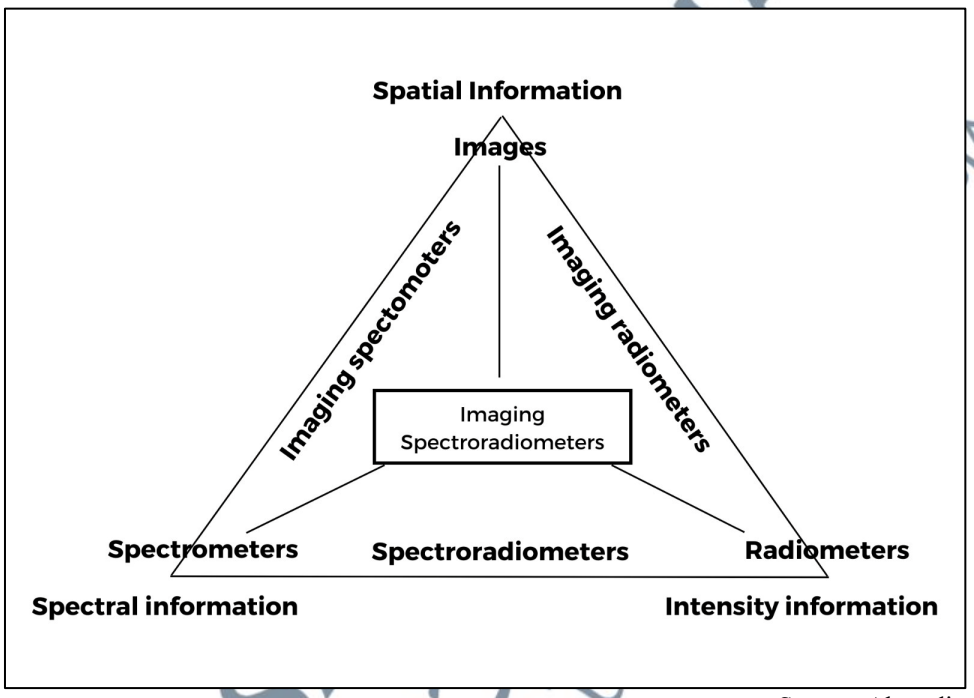

Source: Ahmadja (2006)

Figure 2.14: Different Types of Data That Is Sought and Various Sensors That Are Used for Acquiring the Data in The Hyperspectral Imaging System

Each of these components contains information in multiple dimensions. For instance, there are multiple spectral bands in the sampled volume, which facilitates the analysis extension to the “nth” dimension. The concept of n-dimensional space, often called hyperspace, is used when working with multidimensional systems. Hyperspace is a logical expansion of the 3-D space for analyzing intricate multivariable situations.

In such situations, multivariate image analysis and chemometrics (use of mathematical or statistical methodologies to chemical data) are useful. The chemometric tools are applied to the gemstones when mapped, allowing for the acquisition of chemical, spatial, functional, structural, and even temporal data. This method may provide more comprehensive solutions for some of the challenges faced by the gemological industry today. Nevertheless, color alone does not determine the quality of a ruby stone, which is a qualitative step in determining the grade of ruby stones.

Pan et al. (2019) used statistics to grade gemstones. A total of 120 jadeite-jade (red) samples of varying colors were statistically analyzed. They evaluated the samples with the help of an integral spherical spectrophotometer, X-Rite SP62. They used the K-Means clustering analysis technique from the Statistical Package for the Social Sciences (ver. 2.0) to grade the red jadeite-jade color. In addition to developing an objective and efficient color grade assessment technique, the research used the Fisher discriminant analysis approach to test the classification procedure's viability (Pan et al., 2019). They could classify five different grades of the jadeite-jade red color: Fancy Bright, Fancy Dark, Fancy Intense, Fancy Deep, and Fancy. Because the result is dependent on color rather than the numerical value of the gemstone, this technique has some limitations. Classification of the gemstone based on the light intensity values derived from the sensor is described as its optical properties value.

The GIA is a non-profit institution that is a leader in the knowledge, standards, and education of gems and jewelry. They designed a micro-feature of the ruby chart that includes highly detailed photomicrographs. They highlight the internal features of

the natural, treated, and synthetic rubies that gem traders and gemologists can use as a standard (Renfro et al., 2018).

Apart from that, Gemology Tools Professional is a software that contains approximately 542 gemstone databases. It gathers various gemstone weight estimations, colored stone weight estimations, cabochon weight estimations, gem spectral images, specific gravity calculations, and carat weight charts (Clark, 2022). Jewelry and gemstone appraisers can use the databases in Gemology Tools Professional as references to identify gem characteristics (Clark, 2022). Besides the software, the German Gemological Association compiles and updates gemological tables to identify natural and synthetic gem materials, organic substances, artificial products, and imitations (Boehm, 2021). The layout features 11 columns of properties, starting with a column of ascending RI values conveniently located on the far left of each page. This is followed by birefringence, optic character, density, color, transparency, pleochroism, hardness/cleavage, the gem material's name, and chemical composition (along with crystal system), and, finally, notes on additional characteristics such as structure, fluorescence, inclusions, absorption spectrum features and reaction to hydrochloric acid (Boehm, 2021).

However, the jewelry appraisers will still need to depend on the color spectra provided in Gemology Tools Professional and the gemological tables, a qualitative method that relies on human experience and pictorial ability. Table 2.2 summarizes the operating principles of existing Gemology tools and their limitations in providing optical properties valuations.

Table 2.2: Summary of Existing Gemmology Tools

Type of Gemmology Tool	Operating Principle	Limitation(s)
Loupe, Microscope, and Dichroscope (Liao et al., 2017; Mukherjee, 2012)	Evaluation of a gemstone's clarity, cut, and color using direct observation with the human eye. Highly dependent on pictorial inspection and jewelry appraisal experience.	Prone to human error.
Polarizing microscopy and Raman spectroscopy (Yu et al., 2019)	Analysis of the chemical and physical characteristics as well as the inner structure of a gemstone.	Not a consistent method as it depends on the inner structure of the gemstone.
Laser Ablation–Inductively Coupled Plasma–Mass Spectrometry (LA-ICP-MS) (Abduriyim & Kitawaki, 2006; Sutherland et al., 2019)	Identification of the element composition of a gemstone in order to determine its geographic origin.	Can only be used to determine the origin of a gemstone.
High-Energy Ultraviolet Luminescence (Breeding et al., 2006)	It does not effectively reveal the weak and/or highly detailed patterns as the treatments cause few variations in the fluorescence reactions.	Causes changes in the pattern of a gemstone due to a fluorescent reaction.
DiamondView™ diamond appraisal device (Breeding et al., 2006)	Uses a very high-energy ultra-short-wave (230 nm) UV radiation to induce fluorescence in the diamonds to reveal the growth patterns, which could help in differentiating the natural and synthetic stones.	Can only be used to determine the originality of a gemstone, if it is man-made or synthetic.
Imaging spectroscopy (Del Re, 2006)	Capturing the spectral, spatial, and intensity of a gem to distinguish its color intensity, which is also a qualitative method of gemstone grading.	The results are color-based and do not offer a quantitative value of the gemstones.
Statistical gemstone grading (Pan et al., 2019)	In this study, the researchers statistically analyzed the different colors of 120 jadeite-jade (red) samples. All samples are assessed using an integral spherical spectrophotometer, X-Rite SP62, for classifying the color grade.	The results are color-based and do not offer a quantitative value of the gemstones.
Gemology Tools Professional software (Renfro et al., 2018)	Comprising almost 542 gemstone databases, it gathers various gemstone weight estimations, colored stone weight estimations, cabochon weight estimations, spectral images of gems, specific gravity calculations, and carat weight charts.	Still relies heavily on the appraiser's experience, which is prone to human error.

2.5 Conceptual Framework of CCD and Tomography

2.5.1 Tomography

Signal processing is a rapid technology developed in Industry 4.0. It is an engineering approach that helps interpret the data received from physical events ("IEEE Signal Processing Society," 2018). Many signals like sound, images, and scientific measurements are needed for analyzing, modifying, or synthesizing the data. This technique has improved the communication between biotechnology and social interactions ("IEEE Signal Processing Society," 2018).

One prime example of the signal processing technique is the tomography system. This tomography system is used for viewing 2D or 3D images as a function of time. Figure 2.15 presents the basic block diagram for a tomography system (Abd Rahman et al., 2015).

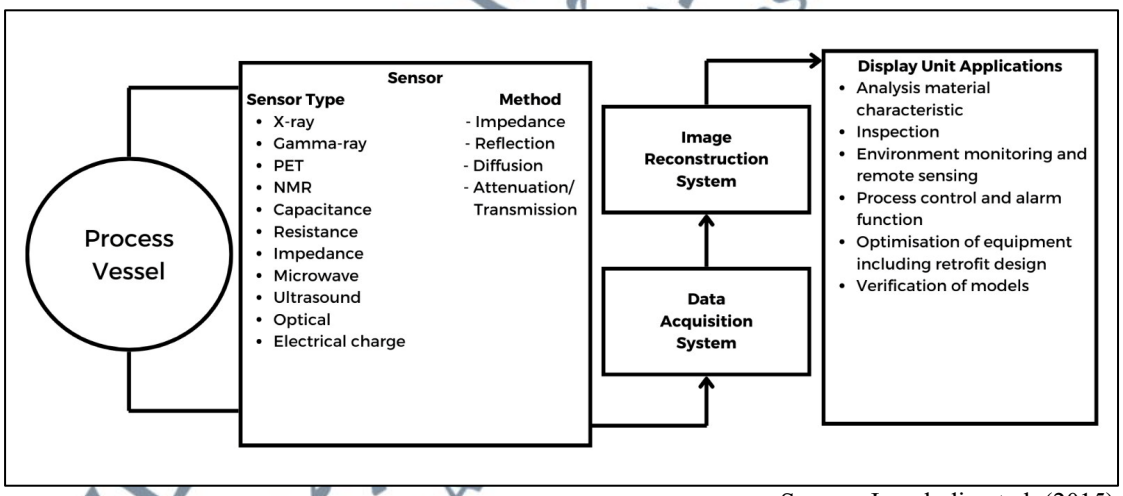

Source: Jamaludin et al. (2015)

Figure 2.15: Block Diagram of a Typical Tomography System

The tomography process includes using non-invasive sensors to capture significant data and generate 2D and 3D images, which help determine the process systems' variable internal properties (Abd Rahman et al., 2015). In the flow industries, these constructed images help identify the vector velocity, flow regime, and concentration distribution (Goh et al., 2016).

This data helps improve the process equipment, assess the existing computational models, simulation processes, and control and monitoring processes (Nassau, 2003). Currently, the tomographic systems are used for obtaining the concentration profiles of the necessary moving components within the measuring section. These are obtained as visual images that can be updated at a rate based on the process being analyzed (Tang et al., 1988).

Tomographic processes have been widely used in the medical field since the 1950s. For example, Computed Tomography (CT or CAT) includes the combination of Computers and X-rays to display images of many organs, bones, and body tissues (Abd Rahman et al., 2015). A comparison of the CAT images to the X-ray images showed that the CAT method offered more detailed images. This technique is also used in many industries for monitoring a pipeline to prevent the splitting of welding defects, media corrosion, cavitation degradation, and material deterioration after a specific time, as these could lead to explosion or leakage-related accidents (Abbaszadeh et al., 2013).

Ultrasonic tomography was developed for handling these issues as it attenuated the ultrasonic energy in the steel pipes. This system is also widely used in the multiphase flow industry, as it is a non-invasive and non-intrusive monitoring system (Cailly et al., 2020). This present study used optical tomography as a sensor to measure output, and

its use as a light-sensitive sensor is discussed in the next section–CCD. Table 2.3 provides a summary of other types of tomography and their characteristics.

Optical tomography is a very effective technique as it is easy to comprehend, inexpensive, and presents a better dynamic response than other radiation-based tomographic techniques like X-ray and Positron emission tomography (Liao et al., 2017). Optical tomography has developed into a feasible new imaging technique in recent years. The benefits of optical sensors are their quick response time, great performance, and uncomplicated architecture (Dharnidharka et al., 2021). This is regarded as an active and linear system that presents reconstructed images that can be directly connected to the visual images that are noted in the transparent areas of the process vessel, thereby outperforming other tomographic imaging techniques. The optical fiber sensors possess a wide bandwidth, allowing high-speed particles to be measured. In the past, the optical tomography (OPT) technique required a transparent section in the pipeline system and offered a high-resolution image (Tang et al., 1988). OPT shows many advantages compared to the hard-field sensors (Mukherjee, 2012), wherein the OPT sensor is independent of the differences in conductivity or permittivity values of the subjects. It also shows a high spatial resolution, which helps acquire a detailed and clear image without revealing any pixels.

Table 2.3: Summary of Other Types of Tomography and Their Characteristics

No.	Types of Tomography System		Characteristics	References
1.	Ultrasonic tomography (UT)		• Image produced using ultrasound waves • Can differentiate the elasticity and density of certain objects very well • Provides quick responses (within seconds) • Can only travel effectively through a medium • Less radiation exposure • Reasonable cost • Multiple pieces of physical data can be obtained using a small power supply	(Asher, 1983; Sallehuddin Ibrahim et al., 2014; Qorbani & Aghdam, 2020)
2.	Electrical tomography	Electrical Resistance Tomography (ERT)	• Based on electrical conductivity (current-voltage correlation) • Measure the resistivity of an object • Able differentiate between phase to produce 2-D and 3-D images • Shorter computational time • Cost-effective	(Holden et al., 1998; Hoyle et al., 2001; Kim et al., 2006; Li et al., 2020; Sher et al., 2016)
3.		Electrical Impedance Tomography (EIT)	• Measure the impedance of an object • Generates less noise due to voltage-based excitation schemes • Low cost • Non-obtrusive • Able to produce a cross-sectional image of multiphase flow systems	(Boone & Holder, 1996; Faia et al., 2020; Mat-Shayuti et al., 2019)
4.		Electrical Capacitance Tomography (ECT)	• Measures the capacitance of an object • Generates a cross-sectional image that depicts the concentration and distribution of dielectric materials in the region of interest (ROI) • Measures the difference in the permittivity of two types of materials • Non-intrusive and non-invasive • Quick response times • Capable of producing cross-sectional images • Cheaper computational cost	(Cui et al., 2015; Lei et al., 2018; Yang et al., 2004)

Table 2.3: Summary of Other Types of Tomography and Their Characteristics

No.	Types of Tomography System	• Characteristics	References
5.	Optical tomography	• Generates images and models using light that is scattered and transmitted around the system • Depends on the intersection of light beams and particle movements • The concept of optical coherence is based on light reflection • Uses low coherence light and ultra-short laser pulses	(Bouma et al., 2022; S. Ibrahim et al., 1999; Shaipanich et al., 2017)
6.	X-ray tomography	• Able to penetrate the internal structure of an object • High-scan speed • Micro-CT provides spatial resolution down to the submicron level	(Liu et al., 2016)
7.	Magnetic resonance imaging tomography	• Uses non-ionising electromagnetic radiation to map the internal structure and functioning parts of an object • Uses radio frequency in the presence of highly-controlled magnetic fields • No risk of exposure • Produces high-quality cross-sectional images • Able to noninvasively analyse optically-opaque multicomponent systems	(Geva, 2006; Katti et al., 2011)
8.	Microwave tomography	• Generates images of dielectric characteristics based on measurements of the dispersed electromagnetic fields created by an object	(Larsen & Jacobi, 1979; Peronnet et al., 1983)
9.	Gamma-ray tomography	• Gamma cameras or PET cameras capture the radiation emitted by radiopharmaceuticals to produce the desired images • Able to penetrate metallic vessels • Capable of scanning large objects • Provides greater flexibility than X-ray imaging • Significantly lower cost	(Bieberle et al., 2013; Duduković et al., 2002)
10.	Neutron tomography	• Neutrons produced from nuclear fission are split into higher and lower energy • High and low-energy neutrons are used to produce images	(Afework et al., 2018; Tengattini et al., 2021; Tudisco et al., 2015)

Table 2.3: Summary of Other Types of Tomography and Their Characteristics

No.	Types of Tomography System	• Characteristics	References
11.	Wire mesh tomography	• Relies on the instantaneous local conductivity of two-phase mixtures • Can efficiently monitor multiphase flows • The multiphase flow characteristics are derived using image reconstruction • A sensor monitors the capacitance or conductance • Conductivity WMT determines the current (or voltage proportional to current) that reflects the local conductivity of fluid • Permittivity WMT assesses the capacitance of the space adjacent to the electrodes proportional to the permittivity of a fluid • Requires a relatively high amount of electrical conductivity	(Banowski et al., 2017; Shaban & Tavoularis, 2017; K. Sun & Li, 2020)

2.5.2 CCD

Soft-field and hard-field sensors are the two types of sensors. The dispersion of material in the assessing volume determines the response of a soft-field sensor (Mukherjee, 2012). Soft-field sensors include magnetic, capacitance, and electrical charge sensors. A hard-field sensor is sensitive to any parameter measured in different positions within the measuring volume. Thus, the measured parameters' distribution inside and outside the measuring area does not affect its sensitivity (Mukherjee, 2012). The CCD (a type of OPT sensor) is classified as a hard-field sensor.

In this study, the researchers used the CCD tomography process to determine the transparency and presence of blemishes in the ruby stones. This non-intrusive and non-invasive technique helps properly assess the object's optical characteristics. Many researchers (Jamaludin, 2016; Jamaludin et al., 2015; Jamaludin, Abdul Rahim, et al., 2016; Jamaludin, Rahim, Rahiman, et al., 2017) used the CCD technique for studying the optical tomography system. According to these studies, the CCD Sony ILX551A works well with a low-power laser diode emitting red light. The main objective of this study is to measure the intensity of the light received by the CCD. Figure 2.16 provides a theoretical understanding of how light penetrates objects of varying transparencies.

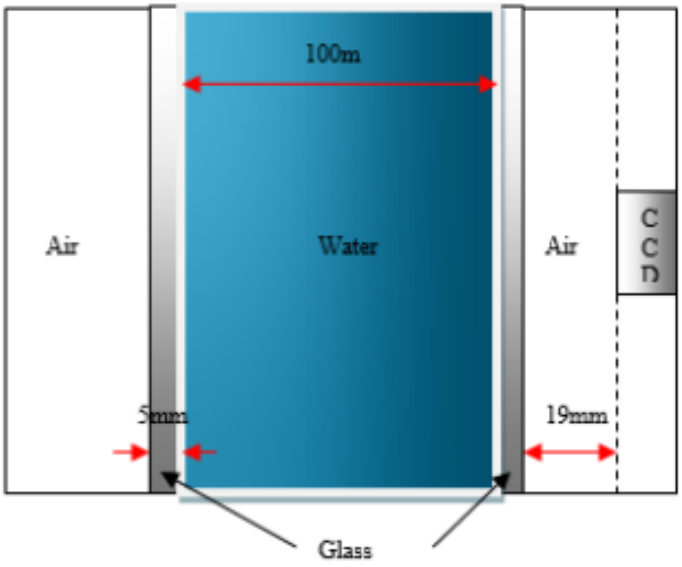

Source: Juliza Jamaludin & Abdul Rahim (2016)

Figure 2.16: Light Penetration Process

The light waves strike the CCD surfaces and are transformed into an electrical voltage output value signal. The CCD voltage value represents the light intensity level. The photon charges received from the light waves are collected by the CCD pixels, such that the more the number of photon charges received by the CCD, the greater the clarity of the gemstones (Jamaludin et al., 2015; Mohd Rahalim et al., 2021).

According to the results presented in these studies, the CCD Sony ILX551A works well with a low-power laser diode (red light source). The CCD optical tomography system can identify the presence of blemishes and transparency of the objects placed in crystal-clear water. The CCD optical tomography technique notes the light intensity that enters the objects, and this value is used for classifying the transparency and presence of blemishes within the object. The above principle is used for determining the intensity of light received by CCD.

The architecture of the CCD sensor is unique; it includes thousands of very small pixels that are responsive to light sources. CCD pixel provides micrometers measurements, allowing thousands of pixels to exist in one device. This type of sensor shows many advantages, like quick detection speed, low noise interference, and high resolution (S. Ibrahim et al., 2012; Jamaludin et al., 2015). Mohd Rahalim et al. (2022) review the application of the CCD tomography system for the gemological industry, where the CCD architecture has been proved to be able to evaluate the optical properties of gemstone since it is very sensitive to light (Mohd Rahalim et al., 2022).

The light signals that strike the CCD surfaces get converted to an electrical voltage output signal. Here, the CCD voltage output value indicates the light intensity level. The photon charges obtained from light are collected by the CCD pixels. The higher the number of photon charges collected by the CCD, the greater the clarity of the gemstones that are being examined (Jamaludin et al., 2015).

Jamaludin et al. (2016) used a CCD linear sensor and a low-power laser diode to capture images of a glass rod, a static solid rod, and a transparent hollow straw placed in crystal-clear water. The tomographic data indicated that the CCD technique could differentiate between the various opacity levels of the various static rods placed in crystal-clear water (Jamaludin, Rahim, et al., 2016; Jamaludin & Abdul Rahim, 2016). In this study, the research aim was to apply the above process for determining the optical properties value of ruby stones based on the CCD voltage output value and the light intensity ratio. The CCD data would be used to develop a mathematical expression that highlights the relationship between the light intensity received by the CCD after penetrating the ruby stone.

2.5.3 Image reconstruction model

Image reconstruction combines data acquired from sensors that have captured images of a subject from various angles and views (Zeng, 2001). As such, the appropriate algorithms are required to solve equations and reconstruct virtual cross-sections to generate the final image (Haneberg, 2004). The most commonly used image reconstruction methods are linear, iterative, and heuristic, of which linear methods are the simplest and fastest. Linear methods commonly use LBP. However, it produces poor image reconstruction for analysis. This method was also used in the early stages of medical tomography (Isaksen, 1996). The drawbacks of LBP include the production of blurry images and complications in compiling scattered images. In such cases, filtering is often used to improve image reconstruction. The filtered back-projection algorithm is well-known to enhance image reconstruction (Zeng, 2001).

As computing loads yield non-linear iterative algorithms that are too slow to process the data, they are not suited for real-time image reconstructions. However, this method makes it easy to model and manage projection noise (Isaksen, 1996). There are two types of heuristic methods: linear and nonlinear. This method is based on the correlation between the trained and measured images (Tapp et al., 2003). Most image analyses rely on pixel values, and simple image analyses use the pixels' mean, minimum, and maximum values. The values of these pixels represent concentration, filling fraction, or packing density (Tapp et al., 2003).

The OPT tomography systems used three types of optical sensor models for their application in sensitive mapping, i.e., optical attenuation, optical path length, and optical path width. Effective measurement of the sensor value in the optical path length technique was based on the interception of a light beam length. There is an increased

probability of the particle intercepting the light beam with an increase in the active light length (Abdul, 1996). Furthermore, the optical attenuation technique includes the absorption and reflectance values of the light beam caused by a blocking object (Sallhuddin Ibrahim, 2000). However, the optical path width sensor modeling includes an obstacle's interruption of the light beam width (Abdul, 1996).

The CCD tomography model comprised two methods. The first was the optical path length method, where the voltage value increases as the particle flow rate increases. Similarly, if many particles intersected the light beam, the voltage would increase (Abdul Rahim & San, 2008). Furthermore, the optical beam may be completely or partially obstructed when opaque objects are transported through the detecting volume. The second model was based on the Lambert-Beer law, which states that optical attenuation occurs in measurement sections with varying optical densities (S. Ibrahim et al., 1999). Owing to the complexity of the mathematical model and since the particle size was greater than the wavelength of the light beam received, the research considered the absorption and refraction attenuation values; however, they neglected the scattering attenuation phenomenon (Idroas, 2004).

Process tomography has extensively used the LBP algorithm, originally developed for x-ray tomography, and it has the advantage of a low calculation cost (Jamaludin et al., 2014). The LBP approach calculates concentration profiles from the measured sensor readings using sensitivity maps developed for individual sensors. S. Ibrahim et al. (1999) proposed a study on different optical sensor configurations that could be used for process tomography. The LBP algorithm calculated the sum of the sensitivity matrixes for every sensor multiplied by the sensor voltage value. The sensitivity matrix for every sensor included one 8 × 8 matrix with 64 numerical values,

most of which were zero. This resulted in 'n' 8 × 8 matrixes, where n represented the no. of projections. This procedure was mathematically described as follows:

$$V_{ij} = \sum_{n=1}^{n=m} V_{S_n} S_n \quad (2.1)$$

Where:

V_{ij} = Voltage distribution in one 8 × 8 matrix

V_{sn} = Voltage for the n^{th} sensor

Sn = Sensitivity map for the n^{th} sensor represented as an 8 × 8 matrix

m = Total number of sensors used.

The matrix was generated after calculating the ratio of the area of the light beam in every pixel to the corresponding pixel's area. For example, if the travel length of the whole pixel beam was 10 mm, the pixel area was seen to be 100 mm^2, the beam area was 10 mm^2, and the sensitivity was 0.1. Each pixel was evaluated independently, and a sensitivity map was then generated using the sum of each pixel's contribution. Jamaludin et al. (2016) used a CCD and the optical tomography system to detect the matter in crystal-clear water after applying the LBP algorithm. In her study, she proposed that this technique could improve the ability of CCD to identify objects that were not opaque. The images were reconstructed based on the orthogonal projection of the laser and CCD results in the pipeline, as shown in Figure 2.17.

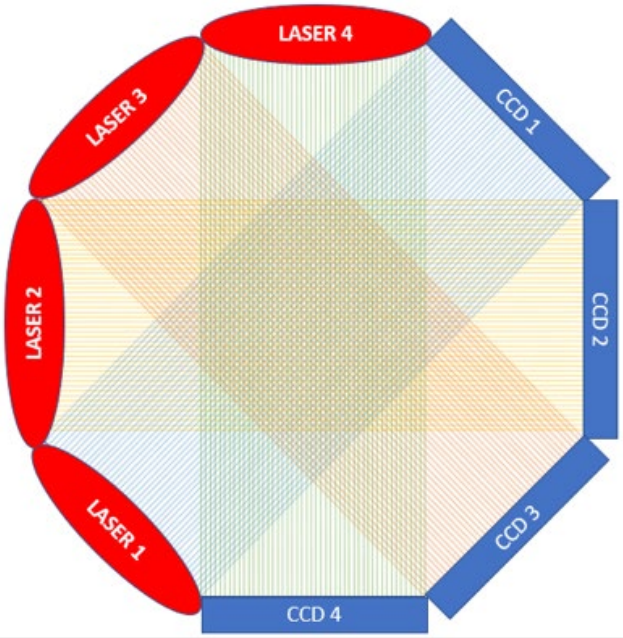

Source: S. Raisin (2020)

Figure 2.17: Arrangement of The CCD Apparatus and The Laser Light Source

The research applied the filtered LBP technique for constructing 3D images using the LabVIEW software. The technique's effectiveness was determined with the help of different objects, such as a transparent rod, a solid rod, and air bubbles. The color intensity increased as the opacity of an item increased. Furthermore, the difference between 3D images, subjected to/ not subjected to the filtering LBP technique was also validated in this study. The use of a threshold operation has been investigated and was found to reduce image artifacts. The flow distribution and fraction of flow components influence the level of thresholding. As a result, adaptive thresholding is frequently required (S. Ibrahim et al., 1999). Figure 2.18 depicts images generated without LBP filtering while Figure 2.19 depicts images generated with LBP filtering. As seen, the images in Figure 2.19 provide a clearer and more accurate position of a static object (Jamaludin, 2016).

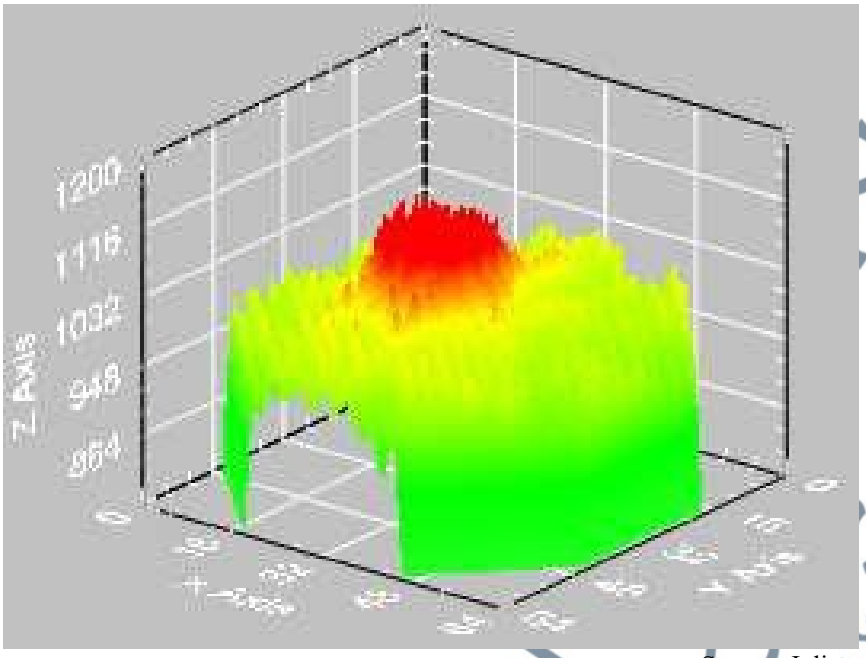

Source: Juliza et al. (2016)

Figure 2.18: Appearance and Location of Static Objects

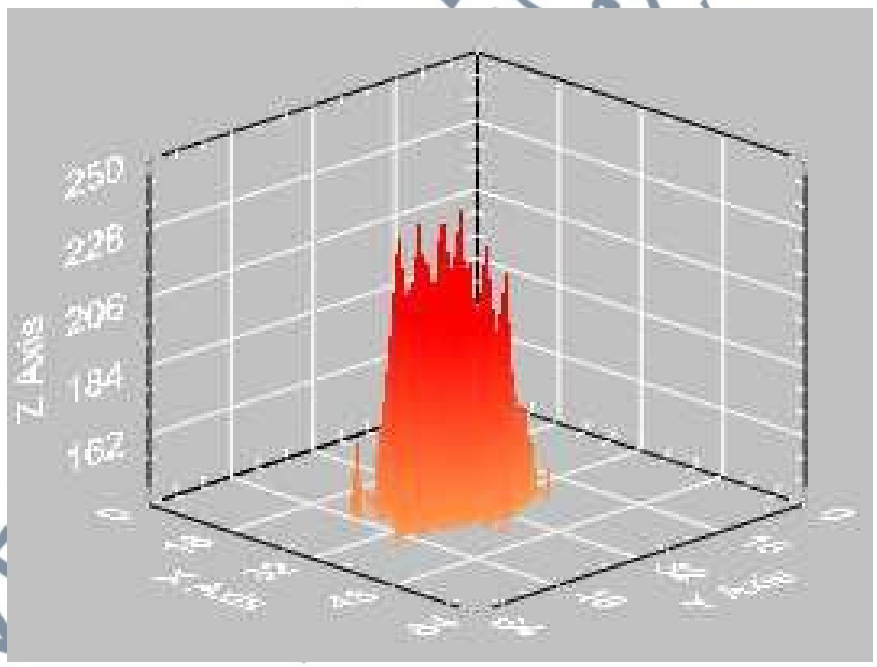

Source: Juliza et al. (2016)

Figure 2.19: Appearance and Location of Static Objects Post-Filtering

The research studied and compared the appearance and the location of different static objects in the above image sets. A hybrid reconstruction algorithm was an alternative approach that could be used instead of the LBP algorithm having a threshold value (Jamaludin, 2016). The sensor voltage output is set to a binary value in the hybrid technique, wherein it is one when the light beam intercepts an item and zero if there is no obstruction. Therefore, this strategy can be used to reduce the impact of smearing and ambiguity. The heuristic technique's correlation between the trained and measurement images is the basis. The mean, lowest, and maximum pixel values are used in simple image analyses. These pixel values represent the image concentration.

In the case of a 2-phase flow imaging process, a novel technique known as the Average Grouping Color can be used to improve the LBP image reconstruction with a smearing effect (Muji et al., 2012). This technique divides the color bar for picture reconstruction into eight groups based on a threshold concept. The value is determined based on the color group once the output value of the sensor has been averaged. Dark colors usually represent solid objects, while less dense objects are usually represented by bright colors (Muji et al., 2012). Artificial neural networks (ANNs) are a new technique that can be used in complicated systems for pattern recognition and trend prediction. Neural Networks (NNs) are described as parallel information processing systems made up of layers of basic neurons (also called nodes or units) linked with one another. The ANNs are designed to reflect the densely connected architecture of the brain and nervous system in animals and humans, with neurons representing the cell bodies and links corresponding to the axons in nature (Dieterle, 2003). Figure 2.20 presents an example of the multilayer feedforward NN using 3 input variables of x_1, x_2, x_3, and a single response variable (y).

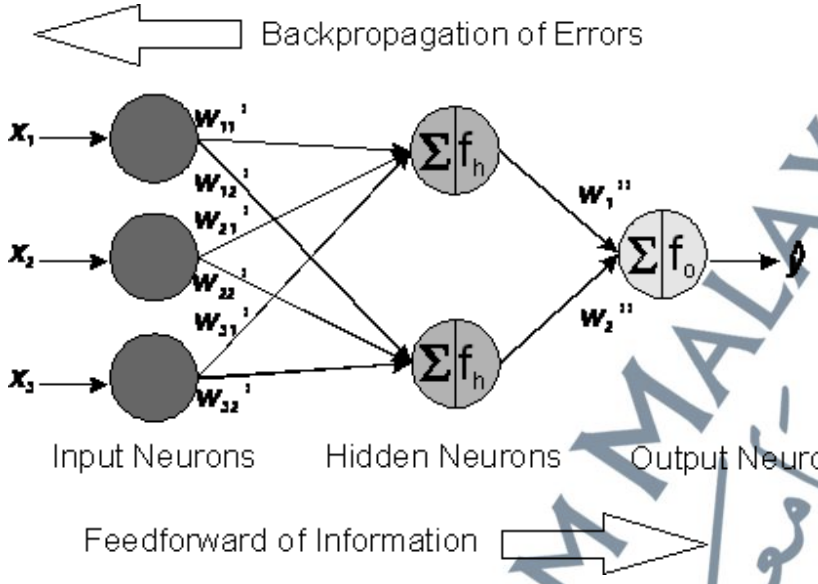

Source: Dieterle (2003)

Figure 2.20: Network Elements in A Multilayer Feedforward Backpropagation Network

The ANN's neurons (or nodes) receive the input signals and generate an individual output based on the weighted sum and nonlinear activation function. These weights are adjusted to achieve learning (Xie et al., 2004). Earlier studies have indicated that the NN can be used to objectively classify the liquid-vapor dispersion data and process the tomography images (Ghosh et al., 2012; Mi et al., 2001; Rosa et al., 2010). A few researchers have made use of the measured or simulated impedance (conductance) signals rather than the ECT input (Ghosh et al., 2012; Hu et al., 2011; Mi et al., 2001; Rosa et al., 2010). Furthermore, most of the extant studies on neural network-based flow identification focus on vertical flows.

Past studies showed that CCD could identify different object transparencies when it is used as the sensor during optical tomography (Jamaludin et al., 2015;

Jamaludin, Rahim, et al., 2016; Jamaludin, Rahim, Rahiman, et al., 2017; Jamaludin & Abdul Rahim, 2016). The three-dimensional image produces a z-value that can recognize the opacity of an object. As such, this present study utilized the LBP algorithm to quantify the standard grading valuation of ruby stones based on their optical properties.